

Scintillation Theory Revisited

Charles L. Rino

June 18, 2025

Abstract

"The Theory of Scintillation *with* Applications in Remote Sensing" was published in 2011. The website <https://chuckrino.com> was started as a forum for discussing remote sensing of electromagnetic (EM) waves propagating through transparent structured media. The underlying phenomenon is electromagnetic (EM) wave propagation in transparent media, specifically the earth's ionosphere and atmosphere. EM waves are vector fields governed by Maxwell's equations. Linear constitutive relations characterize the EM field interactions with the propagation medium. Scintillation refers to irregular variations imparted to signal parameters that have traversed structured regions.

The physical processes that cause structure development comprise an engaging theory in its own right. Propagation theory connects parameterized remote diagnostic observables with complementary parameterized measures of the in situ structure. Parameters can be estimated with established procedures that reconcile diagnostic measurements with the theoretical predictions.

In the decade that has passed since the book was published more refined interpretations have revealed limitations and new applications of the theory. A set of MatLab procedures accompanied the publication. This report is the first part of a review and update of the original publication and MatLab procedures.

1 Introduction

Scintillation is formally a stochastic modulation imparted to electromagnetic (EM) fields propagating in transparent inhomogeneous media. EM fields initiated by the sun and a plethora of other extraterrestrial sources provided the earliest scintillation observations. Following the launch of Sputnik in 1957 artificial earth satellite sources began to supplement natural sources. The Wideband Satellite, launched in 1976, was dedicated to scintillation observations. The first global positioning satellites (GPS) were launched in 1978. When "The Theory of Scintillation *with* Applications in Remote Sensing" Rino [1] (hereafter *Scint-Theory*) was published in 2011, the global navigation satellite system (GNSS) was becoming the primary source of ionospheric structure diagnostics. This

document reviews *ScintTheory* in light of new theoretical insights and new diagnostic applications. Rino and Zavorotny [2, Chapter 29.6 Radio Scintillation History] reviews the history of radio scintillation.

Propagation theory provides the theoretical framework for characterizing the structure imparted to EM fields propagating in structured media. With a formal incorporation of stochastic processes, statistical measures of the evolving fields can be related analytically to statistical measures of the media structure. For real-world applications the transition between structure that admits analytic characterization and structure that can be characterized only with statistical measures must be identified. The desired end result is a complementary set of simulation and diagnostic procedures supported by a unified theory.

The statistical theory summarized in Chapter 3 of *ScintTheory* is confined to propagating fields that subtend a narrow range of propagation angles. The development follows from a *forward propagation equation* (FPE), which is a generalization of widely used multiple phase screen (MPS) split-step integration. The generalization replaces the parabolic propagator normally used for MPS applications with an exact wide-angle propagator. Recent applications of the FPE to HF propagation was demonstrated in two Rino and Carrano companion papers [3] and [4]. A disparity was found between FPE calculations of a narrow HF beam refracted by an ionospheric layer and ray-trace calculations of the beam trajectory. The source of the disparity was an inconsistent application of the unrestricted propagation operator. This document revisits the development in the Rino and Carrano papers to identify FPE limitations and introduce alternative albeit computationally demanding procedures that are well known in acoustic and seismic applications of propagation theory. Whereas theoretical results derived from the restricted FPE fully accommodate GNSS diagnostic measurements, the extension to HF remains a work in progress.

2 Propagation in Inhomogeneous Media

Chapters 1 and 2 of *ScintTheory* introduced a first-order differential equation ¹, which was referred to as the forward propagation equation (FPE). The FPE is a manifestation of the multiple phase screen (MPS) method. All subsequent results in *ScintTheory* followed from the FPE. The theoretical results that comprise the statistical theory of scintillation, as summarized in Chapter 3 of *ScintTheory*, are applicable only to fields that subtend a narrow range of propagation angles, whereas the MPS propagator is unrestricted. This seems to imply that the FPE is more general than the parabolic wave equation. However, applications of the FPE at HF frequencies revealed a disparity between refracted narrow beam fields and ray theory predictions. The source of the disparity was known in scalar acoustic propagation theory. Here we present a more complete development of the material presented in Rino and Carrano [3] to identify the limitations explicitly.

¹Equation (2.2) in *ScintTheory*.

The starting point is Maxwell's equations. We assume that the media structure evolves slowly enough to be *frozen* over typical measurement intervals. Under this assumption Maxwell's equations can be written in the following time-harmonic form with no further limiting assumptions:

$$\nabla \times \mathbf{E} = -i\omega\mathbf{B} \quad (1)$$

$$\nabla \times \mathbf{H} = i\omega\mathbf{D} \quad (2)$$

$$\mathbf{B} = \mu_0\mathbf{H} \quad (3)$$

$$\mathbf{D} = \epsilon_0\bar{\epsilon} \cdot \mathbf{E} = 0. \quad (4)$$

The vector fields \mathbf{E} and \mathbf{H} represent electric and magnetic field intensities. The vector fields \mathbf{D} and \mathbf{B} represent electric and magnetic induction fields, $f = \omega/(2\pi)$ is the temporal frequency in Hz, and ω is the angular frequency in radians per second. The parameters μ_0 and ϵ_0 are fundamental constants that define the speed of light,

$$c = 1/\sqrt{\mu_0\epsilon_0}. \quad (5)$$

The dielectric tensor, $\bar{\epsilon}$, is defined as

$$\bar{\epsilon} = \bar{I} + X\bar{\chi}, \quad (6)$$

where \bar{I} is the identity matrix, $X\bar{\chi}$ is the susceptibility matrix, which is written as a product of a spatially varying scalar, X , and a 3×3 tensor, $\bar{\chi}$. Departures from homogeneity are defined by the frequency-dependent scalar, X . A complete definition of $X\bar{\chi}$ for the standard homogeneous ionosphere is presented in the Rino and Carrano [3] appendix, which includes the Appleton Hartree equations. All the quantities have the implicit time variation $\exp\{i\omega t\}$. The formulation characterizes the spatial evolution of fields initiated by an impressed source field.

From (1) and (3) with substitutions from (2) and (4) a single vector equation for \mathbf{E} can be derived. The vector wave equation follows after substitution of a standard vector identity for $\nabla \times \nabla \times \mathbf{E}$:

$$\nabla^2\mathbf{E}(\mathbf{r}) + k^2\mathbf{E}(\mathbf{r}) = -X(\mathbf{r})\bar{\chi}\mathbf{E}(\mathbf{r}) + \nabla(\nabla \cdot \mathbf{E}) \quad (7)$$

Regarding the divergence, $\nabla \cdot \mathbf{E}$, the textbook "Waves and Fields in Inhomogeneous Media" Chew [5] avoids explicit treatment of the divergence term by accommodating only homogeneous subregions defined by discontinuous boundaries, e. g. layers and discrete scatterers. Within homogeneous subregions $\nabla \cdot \mathbf{E} = 0$. Induced sources on the boundaries support discontinuous field changes. Strictly speaking, only a homogeneous medium can support divergence-free \mathbf{E} and \mathbf{H} fields. For example if we let

$$\bar{\chi} = \mathbf{V}^{-1}\bar{D}\mathbf{V}, \quad (8)$$

where \bar{D} is a diagonal matrix of eigen values and the columns of \mathbf{V} are eigen vectors, substituting $\mathbf{V}^{-1}\mathbf{E}(x, \boldsymbol{\rho})$ into the wave equation with $\nabla \cdot \mathbf{E} = 0$ leads to independent scalar wave equations, which cannot change the direction of the vector fields. Consequently, solutions to the scalar wave equation

$$\nabla^2\psi(\mathbf{r}) + k^2\psi(\mathbf{r}) = -X(\mathbf{r})\bar{\chi}\psi(\mathbf{r}), \quad (9)$$

which conserve total intensity, must be interpreted as unspecified projections of the measurable vector field.

To facilitate numerical exploration of the scalar wave equation, structure variation will be confined to the xy plane, with no variation along the z axis whereby

$$\nabla^2\psi(x, y) + k^2\psi(x, y) = -k^2X(x, y)\psi(x, y). \quad (10)$$

For ionospheric profiles

$$X(x, y) = 4\pi N_e(x, y)/(r_e k^2) \quad (11)$$

where N_e is the electron density and $r_e = 2.819740289 \times 10^{-15}$ m is the classical electron radius. Directed propagation will be defined with respect to the x axis. Consider an initiating field

$$\psi_0(y) = \int \hat{\psi}_0(\kappa) \exp\{-i\kappa y\} \frac{d\kappa}{2\pi}. \quad (12)$$

Substitution into (10) will show that

$$\psi(x, y) = \int \hat{\psi}_0(\kappa) \exp\{\pm ik\sqrt{1 - (\kappa/k)^2}x\} \exp\{i\kappa y\} \frac{d\kappa}{2\pi} \quad (13)$$

$$= \int \hat{\psi}_0(\kappa) \exp\{\pm i[k\sqrt{1 - (\kappa/k)^2}x + \kappa y]\} \frac{d\kappa}{2\pi} \quad (14)$$

satisfies the homogeneous equation. The second form emphasizes the interpretation of freely propagation fields as independently propagating plane waves defined by the wave vector

$$\mathbf{k} = [\pm k_x(\kappa), \kappa] \quad (15)$$

$$k_x(\kappa) = k\sqrt{1 - (\kappa/k)^2} \quad (16)$$

At this point κ is unrestricted, although the sign of $k_x(\kappa)$ must be chosen so that evanescent contributions from $|\kappa| < k$ are damped.

2.1 Induced Source Methods

Induced sources are manifestations of the Huygens-Fresnel principle. Using the formal Green's function property

$$\nabla^2 H(x, y) + k^2 H(x, y) = -\delta(x - x', y - y'), \quad (17)$$

solutions to the scalar wave equation satisfy the integral equation for

$$\begin{aligned} \psi(x, y) = & \psi_0(x, y) - k^2 \iint \psi(x', y') X(x', y') \\ & \times H(x - x', y - y') dx' dy', \end{aligned} \quad (18)$$

which includes the source field, $\psi_0(x, y)$, explicitly. The structure contributions are effectively induced sources, which connect every point in the propagation space potentially with every other point. Solving the integral equations amounts to determining induced sources that reconcile all the interactions.

The Fourier transformation

$$\int H_0^{(1)}(k\rho)/(4i) \exp\{-ik\kappa y\} dy = \frac{1}{2i} \frac{\exp\{ikg(\kappa)|x|\}}{kg(\kappa)} \exp\{ik\kappa y\}, \quad (19)$$

follows from the Weyl representation

$$\int H_0^{(1)}(k\rho)/(4i) \exp\{-ik\kappa y\} dy = \frac{1}{2i} \frac{\exp\{ikg(\kappa)|x|\}}{kg(\kappa)} \exp\{ik\kappa y\}. \quad (20)$$

Using (20), (18) can be transformed to the spatial Fourier domain

$$\begin{aligned} \widehat{\psi}(\kappa; x) = & \widehat{\psi}_0(\kappa; x) - k^2 \int_0^\infty \int \psi(x', y') X(x', y') \exp\{-ik\kappa y'\} dy' \\ & \times \frac{1}{2i} \frac{\exp\{ikg(\kappa)|x - x'|\}}{kg(\kappa)} dx'. \end{aligned} \quad (21)$$

At this point the summation of waves propagating in the positive (forward) and negative (backward) x directions must be treated explicitly. Two coupled forward and backward equations can be derived. The forward approximation neglects backward propagating waves initiated where $x' > x$:

$$\begin{aligned} \widehat{\psi}^+(\kappa; x) = & \widehat{\psi}_0(\kappa; x) - k^2 \int_0^x \int \psi^+(x', y') X(x', y') \exp\{-ik\kappa y'\} dy' \\ & \times \frac{1}{2i} \frac{\exp\{ikg(\kappa)(x - x')\}}{kg(\kappa)} dx'. \end{aligned} \quad (22)$$

For a small forward increments

$$\begin{aligned} \widehat{\psi}(\kappa; x + \Delta x) = & \widehat{\psi}(\kappa; x) \exp\{ikg(\kappa)\Delta x\} + \\ & \frac{ik}{2g(\kappa)} \int_0^{\Delta x} \left[\int \psi(x + x', y') X(x + x', y') \right. \\ & \left. \times \int \psi(x + x', y') X(x + x', y') \right] dx'. \end{aligned} \quad (23)$$

The derivation here follows the development in Rino and Carrano [3]. The problem is no fully consistent evaluation of the term in square brackets will

preserve the implied additive separation of propagation and media-interaction terms. As Louis Fishman has put it, the equations

$$\begin{aligned} \frac{\partial \widehat{\psi}(\kappa; x)}{\partial x} &= ikg(\kappa) \left[\psi(\kappa; x) + 1/(2g(\kappa)^2) \int \psi(x, y') \right. \\ &\quad \left. \times X(x, y') \exp\{-ik\kappa y'\} dy' \right] \end{aligned} \quad (24)$$

$$\begin{aligned} \frac{\partial \psi(x, y)}{\partial x} &= \Theta \psi(x, y) + \\ &\quad k^2 \int H_0^{(1)}(k|y' - y|)/(4i) \psi(x, y') X(x, y') dy' \end{aligned} \quad (25)$$

where $\Theta \psi(x, y)$ represents an incremental free propagation step, are just plain wrong! At best, the FPE defined as

$$\frac{\partial \psi(x, y)}{\partial x} = \Theta \psi(x, y) - i \frac{k}{2} X(x, y) \psi(x, y). \quad (26)$$

can be applied reliably only when the parabolic form of the propagation operator is used. Bremmer series applications [6], have yet to produce tractable algorithmic results.

2.2 Factorization Methods

An alternative approach to constructing solutions to (10) uses a formal factorization. Rewriting the Laplacian as a differential operator,

$$\nabla^2 = \partial^2 / \partial x^2 + \nabla_{\perp}^2, \quad (27)$$

identifies the x axis as a propagation reference. The differential operator form of the wave equation,

$$\left(\frac{\partial^2}{\partial x^2} + \nabla_{\perp}^2 + k^2 K(x, y)^2 \right) \psi(x, y) = 0, \quad (28)$$

where

$$K(x, y)^2 = I + X(x, y), \quad (29)$$

can be formally factored to as

$$\begin{aligned} &\frac{\partial^2}{\partial x^2} + \nabla_{\perp}^2 + k^2 K(x, y)^2 \\ &= \left(\frac{\partial}{\partial x} - i (\nabla_{\perp} + k^2 K(x, y)^2)^{1/2} \right) \\ &\quad \times \left(\frac{\partial}{\partial x} + i (\nabla_{\perp} + k^2 K(x, y)^2)^{1/2} \right). \end{aligned} \quad (30)$$

The factorization is strictly valid only if the factored components commute, which would eliminate variation along the propagation direction. However, commutation equivalence is necessary only over are integration steps.

The operator factorization form of the forward propagation equation is

$$\left(\frac{\partial}{\partial x} - i(\nabla_{\perp} + k^2 K(x, y))^{1/2}\right)\psi(x, y) = 0. \quad (31)$$

Approximating the square root operator with the first term in a Taylor series expansion leads to the parabolic wave equation or Feit-Fleck approximation [7], which is equivalent to the FPE with the propagation operator replaced by its parabolic form. A formal operator extension to propagation in inhomogeneous media has the general form

$$\psi(x, y) = \int \widehat{\psi}(x; \kappa) \exp\{i\Omega(x; \kappa, K(x, y))\} \exp\{-i\kappa(y - y')\} \frac{d\kappa}{2\pi}, \quad (32)$$

where $\Omega(x, y; \kappa, K(x, y))$ is the spectral-domain counterpart of the square-root operator developed in a series of papers by Fishman [8] [9] [10]. An intuitively applying approximation

$$\Omega(x; \kappa, K(x, y)) = \sqrt{K(x, y)^2 - (\kappa/k)^2}x, \quad (33)$$

can be applied over incremental slabs. The approximation was rediscovered in acoustics by [11]. However, the y variation precludes efficient FFT evaluation, which makes evaluation very time consuming.

2.3 Parabolic Differential Equation Methods

The square root operator can be approximated by implementing analytic approximations to the square-root function. The approximation is improved by substituting $\psi(x, y) = \exp\{ikx\}U(x, y)$ in the operator form of the wave equation:

$$\left(\frac{1}{k^2} \frac{\partial^2}{\partial x^2} - 1 + K(x, y)^2 + \nabla_{\perp}^2/k^2\right)U(x, y) = 0. \quad (34)$$

Following Collins, [12], the PDE can be written as

$$\frac{\partial U(x, y)}{\partial x} = ik \left(-1 + \sqrt{1 + X_P}\right)U(x, y) \quad (35)$$

where

$$X_P = K(x, y)^2 + \nabla_{\perp}^2/k^2. \quad (36)$$

The Pade approximation, which treats X_P as a complex variable, is defined in terms of precalculated coefficients such that

$$-1 + \sqrt{1 + X_P} \simeq \sum_{j=1}^n \frac{\alpha_{j,n} X_P}{1 + \beta_{j,n} X_P}. \quad (37)$$

A split-step solution is implemented with phase corrections,

$$u(x + \Delta x) = \exp\{ik\Delta x(-1 + \sqrt{1 + X_P})\}u(x), \quad (38)$$

which leads to the replacement of the summation by a product form

$$\prod_{j=1}^n \frac{1 + \lambda_{j,n} X_P}{1 + \mu_{j,n} X_P}. \quad (39)$$

Recognizing that X_P contains second derivatives, the coefficients are chosen to ensure that the differential-equation solution is stable and accurate. The PDE method has produced accurate forward propagation solutions. However, selections of coefficients and sampling is problem specific.

The book "Parabolic equation methods for electromagnetic wave propagation," by Levy [13] presents a complete treatment of parabolic wave equation (PWE) methods including stochastic structure, and boundaries.

2.4 Eigenvector Methods

As demonstrated in Collins and Segman [12], the most demanding inhomogeneous media problems can be implemented with the Pade approximation. However, there is a way to construct an exact solution to the forward approximation

$$\frac{\partial \psi(x, y)}{\partial x} = ikQ(x, y)\psi(x, y),$$

where

$$Q = k\sqrt{1 + X + \nabla_{\perp}^2/k^2}. \quad (40)$$

Following [14], consider the formal vector matrix solution

$$\vec{\psi} = \exp\{ik\Delta x \overleftarrow{Q}\} \vec{\psi} \quad (41)$$

where \overleftarrow{Q} is a matrix square root. To interpret the matrix operator \overleftarrow{Q} , let

$$\rho_n = \exp\{2\pi in/N\}, \quad (42)$$

which is an eigenvector or the matrix form of the discrete Fourier transform (DFT):

$$\begin{aligned} \overleftarrow{R} &= [\rho_n^m] \quad n \Rightarrow \text{col}, m \Rightarrow \text{row} \\ \overleftarrow{R} \vec{\psi} &, \end{aligned} \quad (43)$$

where $\overleftarrow{R}' \overleftarrow{R} = \text{diag}(1/N)$. It follows that with

$$\overleftarrow{K} = -\text{diag}((\kappa_n/k)^2) \quad (44)$$

The matrix argument of the square root can be written as

$$\overleftarrow{Q} = \sqrt{\overleftarrow{R}'\overleftarrow{K}\overleftarrow{R}/N + \text{diag}(1 + X_y)} \quad (45)$$

There is an exact solution for $X_y = 0$. Rewriting \overleftarrow{Q} as

$$\overleftarrow{Q} = \sqrt{\overleftarrow{R}'(\overleftarrow{K} + \overleftarrow{I})\overleftarrow{R}/N} \quad (46)$$

the eigen vectors of

$$\overleftarrow{Q}^2 = \overleftarrow{R}'(\overleftarrow{K} + \overleftarrow{I})\overleftarrow{R}/N \quad (47)$$

are the column vectors of $\overleftarrow{R}/\sqrt{N}$. A formal matrix solution that advances any starting field can be constructed as follows

$$\overrightarrow{\psi} = \overleftarrow{R} \left(\left(\overleftarrow{R}'\overrightarrow{\psi}_0 \right) \exp \left\{ -k\Delta x \sqrt{\text{diag}(1 - (\kappa_n/k)^2)} \right\} \right); \quad (48)$$

which can be rewritten as

$$\overrightarrow{\psi} = \left(\overleftarrow{R}'\overrightarrow{\psi}_0 \right) \exp \left\{ -k\Delta x \sqrt{\text{diag}(1 - (\kappa_n/k)^2)} \right\} \overleftarrow{R} \quad (49)$$

The computation follows from an eigenvector decomposition of \overleftarrow{Q}^2

$$\overleftarrow{Q}^2 = \overleftarrow{\Xi}'\overleftarrow{\Lambda}\overleftarrow{\Xi}. \quad (50)$$

The same eigenvectors define \overleftarrow{Q}

$$\overleftarrow{Q} = \overleftarrow{\Xi}'\sqrt{\overleftarrow{\Lambda}}\overleftarrow{\Xi}' \quad (51)$$

The final solution is

$$\overrightarrow{\psi} = \overleftarrow{\Xi}' \exp\{ik\Delta x \sqrt{\overleftarrow{\Lambda}}\} \overleftarrow{\Xi}\overrightarrow{\psi}_0 \quad (52)$$

As a consistency check for free space

$$\text{diag}(\overleftarrow{\Lambda}) = \sqrt{1 - (\kappa_n/k)^2}, \overleftarrow{\Xi} = R/\sqrt{N}. \quad (53)$$

In effect, the complexity of implementing the Pade approximation has been traded for the complexity of computing the eigenvectors of a large matrix. For exploration purposes, the ease of implementation make eigenvector solutions very attractive. However, the eigenvector computation is prohibitively time consuming for range-dependent structure.

2.5 Ray Optics

Whether FPE, PDE, or OHE solutions are implemented, other than internal consistency it is desirable to have a exact result for verification. With $\bar{\chi} = I$, the formally exact defining equation is

$$\nabla^2 \mathbf{E} + k^2 \mathbf{E} = \nabla(\nabla \cdot \mathbf{E}) - k^2 X \mathbf{E}. \quad (54)$$

Ray optics is based on the assumption that the field associated with a propagating field can be approximated locally as single plane wave with a slowly vary amplitude and a smoothly varying phase. Following the development in Born and Wolf [15, Chapter 3.2], $\mathbf{E}(\mathbf{r})$ is approximated as

$$\mathbf{E}(\mathbf{r}) = \tilde{\mathbf{E}}(\mathbf{r}) \exp\{ik\vartheta(\mathbf{r})\}. \quad (55)$$

Inserting (55) into the vector wave equation and retaining only terms that are first-order in ΔX leads to the defining equation

$$(\nabla\vartheta)^2 = n^2, \quad (56)$$

where

$$n^2 = 1 + X. \quad (57)$$

The identification of n as a refractive index follows from the definition

$$\nabla\vartheta = \mathbf{n} \quad (58)$$

where $\vartheta = k\mathbf{n} \cdot \mathbf{r}$. Wavefronts are defined by contours of constant ϑ . If s represents distance along a *ray*, normal to $\nabla\vartheta$, the defining equation can be rewritten as

$$n \frac{d\mathbf{r}}{ds} = \nabla\vartheta. \quad (59)$$

Eliminating ϑ , leads to the ray equation

$$\begin{aligned} \frac{d}{ds} \left(n \frac{d\mathbf{r}}{ds} \right) &= \nabla n \\ \frac{d^2 \mathbf{r}}{ds^2} + \frac{dn}{nds} \frac{d\mathbf{r}}{ds} &= \frac{\nabla n}{n}. \end{aligned} \quad (60)$$

Let

$$\boldsymbol{\tau} = \frac{d\mathbf{r}}{ds}, \quad (61)$$

whereby

$$\frac{d\boldsymbol{\tau}}{ds} + \frac{dn}{nds} \boldsymbol{\tau} = \frac{\nabla n}{n} \quad (62)$$

$$\frac{d\boldsymbol{\tau}}{ds} + \mathbf{s} \cdot \left(\frac{\nabla n}{n} \right) \boldsymbol{\tau} = \left(\frac{\nabla n}{n} \right), \quad (63)$$

where \mathbf{s} is a unit vector along the ray direction. The defining ray equations are fully three dimensional and impose no constraint on the structure other than a self checking smoothness. Reflecting boundaries are readily accommodated.

A complete treatment of ray theory and its extension to vector fields is demanding and leads to advanced mathematical procedures. For example, the ray theory in the seminal text "The propagation of radio waves," by Budden [16] is not presented until Chapter 14. The implementation of the Haselgrove equations requires variational calculus methods Colman [17]. However, for our purposes here an implementation of the ray equations here will suffice.

3 Examples

3.1 Ray Trace

A two-dimensional propagation calculation is defined by a height, a propagation distance, a starting field, a specification of X and frequency, f . An absorbing upper boundary accommodates escaping energy. A reflecting surface or implementation of the forward boundary method described in Rino and Carrano [4] reflects fields at the lower boundary. Current implementations of the PDE and OHE solutions accommodate conducting boundary surfaces with Dirichlet boundary conditions. For exploration a spherical earth propagation environment was implemented. Figure 1 shows the refractive index at 10 MHz for a Chapman layer at 300 km. Rays traced from the source at 50 km are overlaid. A direct implementation of (60) modified to reflect rays from a smoothly varying boundary surface was used to calculate the ray paths. Altitude is measured along normal radials from the surface height defined by a function of y and z . The refractive index for a layer at a fixed radial distance is z dependent. The use of the z axis as the propagation reference for display is an FPE legacy.

3.2 FPE

Although the complete propagation grid was used for the FPE simulations in Rino and Carrano [3], [4], SSPDE and OHE applications require significantly more computation. Consequently, a truncate propagation space was used. The upper frame of For reference, Figure 2 shows the FPE field intensity for beam propagation into a refracting Chapman layer. A ray initiated at the 20 km source height along the measured beam peak direction is overlaid (white). The lower frame shows the spectral intensity with the ray trace direction overlaid. The upper frame in Figure (3) shows the total intensity of the FPE field, which is invariant as long as the field is confined to the propagation space. The loss at the surface reflection is caused by the shift-map implementation of the boundary variation. The lower frame shows the spectral domain peak intensity with the ray direction overlaid, which varies in response to induced waveform variations. For a concentrated beam we expect the trajectory of the peak

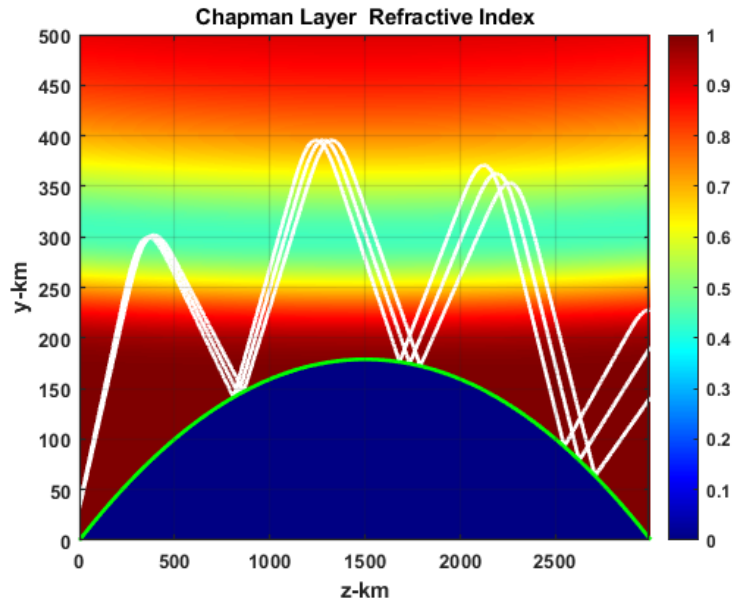


Figure 1: Chapman layer with rays launched from 50 km overlaid.

intensity to coincide with the ray launched along the ray direction. However, as consistently observed, FPE propagation in highly refractive environments underestimates refraction. Without the ray trace for comparison the error might not be noticed.

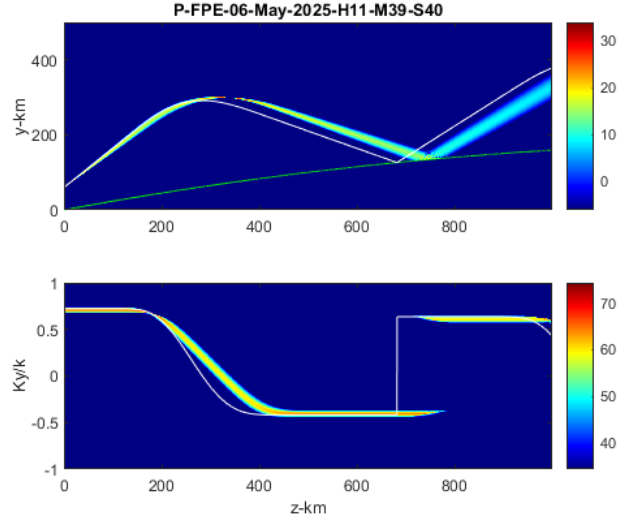


Figure 2: Upper frame is FPE beam intensity with ray trace overlaid. Lower frame shows. Lower frame shows spectral intensity plotted against normalized wavenumber. Ray direction is overlaid.

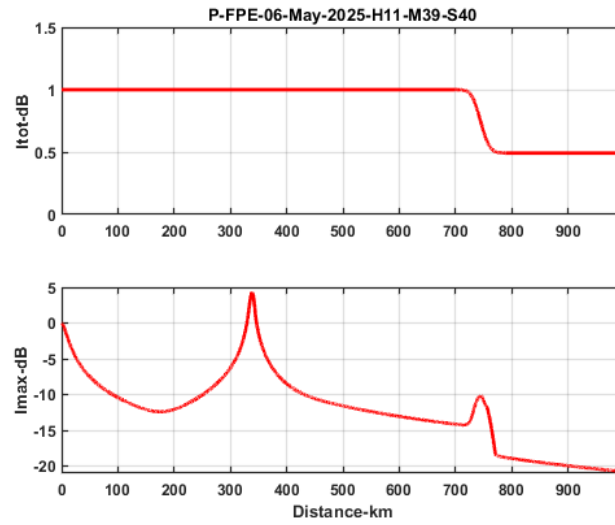


Figure 3: Upper frame shows FPE total intensity. Lower frame shows peak intensity.

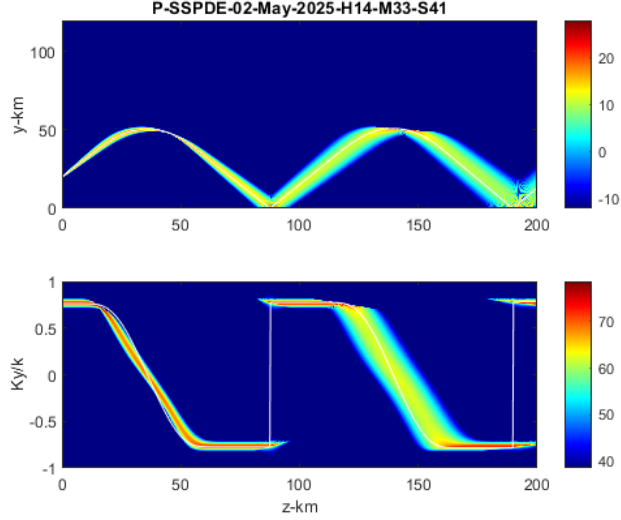


Figure 4: Upper frame is SSPDE beam intensity with ray trace overlaid. Lower frame shows spectral intensity plotted against normalized wavenumber. Ray direction is overlaid.

3.3 SSPDE

Figures 4 and 5 summarize an SSPDE simulation of the Chapman layer environment with a plane conducting layer. The plane conducting layer is used because the solution is formally exact. The upper frame in 4 summarizes the beam intensity with the ray trace overlaid. The lower frame shows the spectral intensity with the ray direction overlaid. Whereas the spatial domain peak aligns almost perfectly with the ray trace, the spectral domain peak deviates from the direction of the ray path. This is attribute to the asymmetry of beam as it forms a caustic beyond the point of inflection. Because the surface reflection is symmetric about the normal direction the ray path direction coincides with the peak. Figure 5 shows the integrated intensity and the beam peak intensity, which increases and decreases in response to induced beamwidth changes. The vertical sampling is 12 per wavelength, 6 samples per wavelength along the propagation direction, and 8 Pade coefficients. The over sampling and the number of Pade coefficients was determined by trial and error.

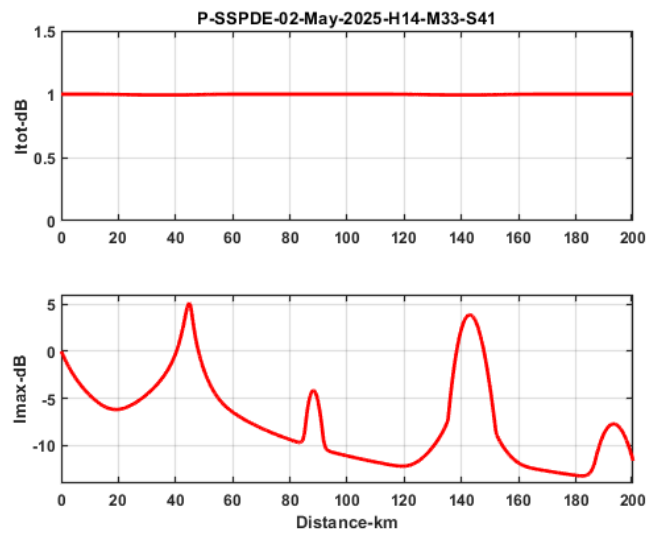


Figure 5: Upper frame shows SSPDE total intensity. Lower frame shows peak intensity.

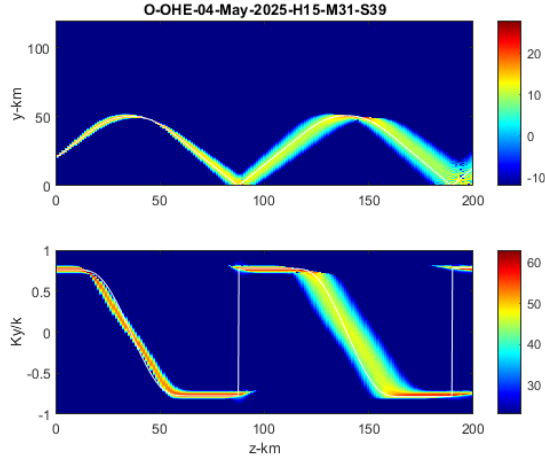


Figure 6: Upper frame is OHE beam intensity with ray trace overlaid. Lower frame shows spectral intensity plotted against normalized wavenumber. Ray direction is overlaid.

3.4 OHE

Figures 6 and 7 summarize the OHE calculation. The OHE calculation is performed with the same critical sampling used for the FPE calculation. Although oversampling is unnecessary for OHE, the eigenvector computation is computationally demanding. However, in a transversely inhomogeneous medium only one evaluation is needed. It is encouraging that the SSPDE and OHE results are identical, including the departure of the ray direction from the spectral domain peak through the caustic formation. It also shows that the SSPDE oversampling is driven by the Pade approximation not evanescent fields.

Belyaev et. al [14] computed the refraction of a beam injected into a neutral layer, which effectively trapped the beam. Figure shows a similar calculation at 10 MHz. The overlaid ray trace required height and direction adjustments to achieve agreement with the wave intensity peak. As with the Chapman layer the ray angle shows significant departures from the wave spectrum peak.

3.5 Commutation limitation

It is generally argued that although factorization methods are strictly valid only in transversely inhomogeneous environment variations that are slow compared to computation intervals can be accommodated. It has been demonstrated that the range dependence imposed by a layer at a constant radial distance a more stringent test is realized by a neutral gaussian lens, generated by a truncated gaussian layer as shown in Figure 10 shows the refractive index of a neutral Gaussian lens with three parallel rays overlaid. The lens action is realized by uniform incident illumination rather than the curvature imposed by a compact

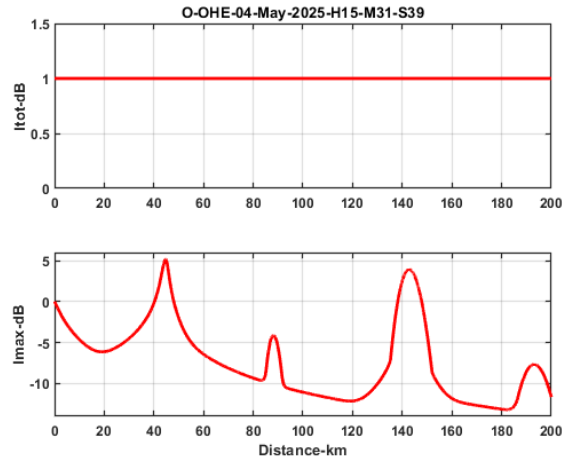


Figure 7: Upper frame shows SSPDE total intensity. Lower frame shows peak intensity.

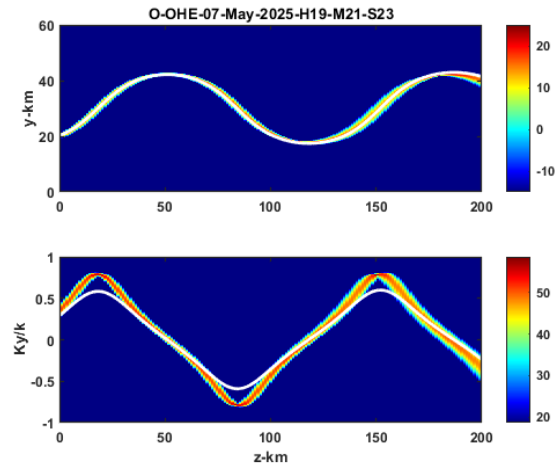


Figure 8: Upper frame is beam injected into a neutral Gaussian layer forming waveguide like propagation. The lower frame show the spectral domain peak with the ray direction overlaid.

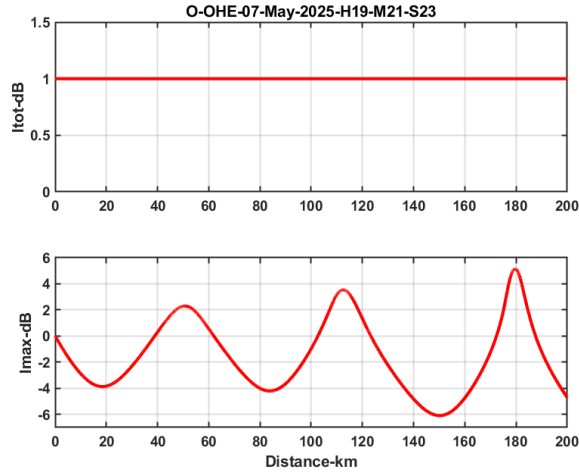


Figure 9: Upper frame shows OHE total intensity. Lower frame shows peak intensity.

source. A common technique for generating a more uniform illuminating field is beam simulation [18], which is a superposition parallel beams. As a test of the refraction a superposition of two parallel beams was used. Figure 11 shows the spatial and spectral domain intensities of the two-beam superposition with the ray trace overlaid. The agreement between the ray trace and beam central crossings show that the range variations had no impact on the calculation.

4 Summary and Conclusions

Whereas tractable EM forward marching algorithms can be constructed for near line-of-sight propagation in the VHF to S-Band frequency range, the extension to lower frequencies developed in our papers [3] and [4] produces results that must be used guardedly. More than underestimating the refraction predicted by ray tracing, there is no fully consistent way to construct vector fields from independently scalar wave computations. The safest procedure is to apply SSPDE to scalar wave equations with the refractive index precomputed mode refractive indices using the Appleton Hartree equations guided by ray trace computations and their extension to full-field approximations.

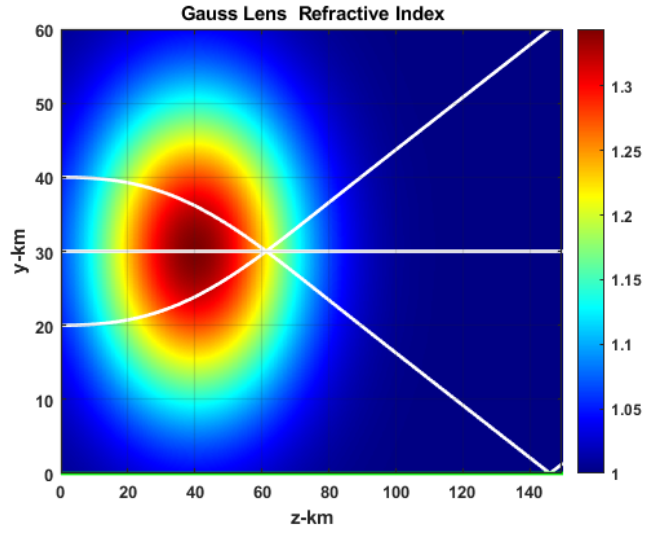


Figure 10: Refractive index of neutral Gaussian lens with parallel rays overlaid.

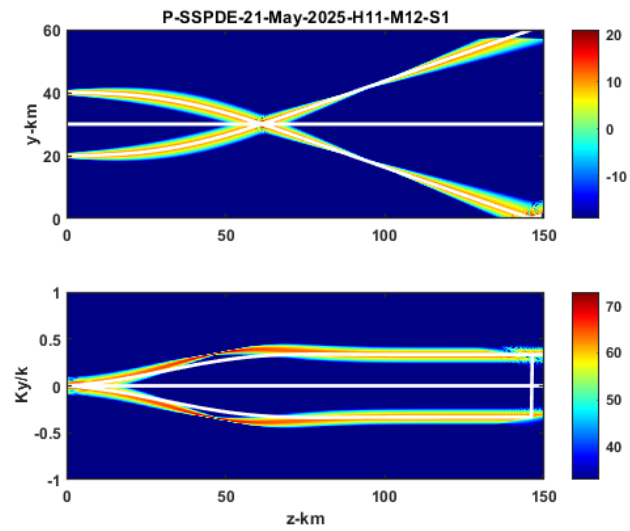


Figure 11: Upper frame shows OHE total intensity. Lower frame shows peak intensity.

References

- [1] Charles L. Rino. *The Theory of Scintillation with Applications in Remote Sensing*. Wiley, 2011.
- [2] Philip Wilkinson, Paul S. Cannon, and W. Ross Stone. *100 Years of the International Union of Radio Science*. URSI, 2021.
- [3] C. Rino and C. Carrano. A vector theory for forward propagation in a structured ionosphere. *Journal of Atmospheric and Terrestrial Physics*, 2021. doi.org/10.1016/j.jastp.2021.105558.
- [4] C. Rino and C. Carrano. A vector theory for forward propagation in a structured ionosphere with surface reflections. *Journal of Atmospheric and Terrestrial Physics*, 2021. doi.org/10.1016/j.jastp.2021.105740.
- [5] Weng Cho Chew. *Waves and Fields in Inhomogeneous Media*. A Van Nostrand Renhol, 1990.
- [6] H. Bremmer. The w.k.b. approximation as the first term of a geometric-optical series. *Philips Research Reports*, 4:189–, 1949.
- [7] M. D. Feit and Jr. J. A. Fleck. Light propagation in graded index fibers. *Applied Optics*, 17:3990–3998, 1978.
- [8] Louis Fishman, John J. McCoy, and Stephen C. Wales. Factorization and path integration of the helmholtz equation: Numerical algorithms. *Acoustical Society of America Journal*, 81, 1987. doi:10.1121/1.394542.
- [9] Louis Fishman and John J. McCoy. Derivation and application of extended parabolic wave theories. i. the factorized helmholtz equation. *Journal of Mathematical Physics*, 25, 1984. doi.org/10.1063/1.526149.
- [10] Louis Fishman and John J. McCoy. Derivation and application of extended parabolic wave theories. ii. path integral representations. *Journal of Mathematical Physics*, 25, 1984. doi.org/10.1063/1.526150.
- [11] Vladimir E. Ostashev, Michael B. Muhlestein, and D. Keith Wilson. Extra-wide-angle parabolic equations in motionless and moving media. *J Acoustical Society of America*, 145(2):1031–1047, 2003. doi.org/10.1121/1.5091011.
- [12] Michael D. Collins and William L. Siegmann. *Parabolic Wave Equations with Applications*. Springer, 2019.
- [13] Mireille Levy. *Parabolic equation methods for electromagnetic wave propagation*. The Institution of Electrical Engineers London, 2000.
- [14] Mikhail A. Belyaev, Jeffrey Banks, and Thomas Chapman. Exact wave solver for nonparaxial laser beam propagation. *Phys. Plasmas*, 31, 2024. doi: 10.1063/5.0198523.

- [15] M. Born and E. Wolf. *Principles of Optics*. Cambridge University Press, 1999.
- [16] K. G. Budden. *The Propagation of Radio Waves*. Cambridge University Press, Cambridge, 1985.
- [17] Christopher Coleman. Ionospheric ray tracing equations and their solution. *The Radio Science Bulletin*, 39, 2008.
- [18] Hoc D. Ngo and Charles L. Rino. Application of beam simulation to scattering at low grazing angles 1. methodology and validation. *Radio Science*, 29(6), 1994.